Seismic deformation at the Alban Hills volcano during the 1989-1990 seismic sequence

Giulio Selvaggi and Francesca D'Ajello Caracciolo
Istituto Nazionale di Geofisica, Roma, Italy

Abstract
We analysed the one-year-long seismic swarm at the Alban Hills volcano which occurred during 1989-1990. We portray spatial distribution of seismic moment release, better delineating the activated volume during the swarm. The seismic structure is imaged as a 7-km long, 3-km wide, and 3-km thick volume, located between 2 and 5 km depth, and NW-SE striking. Fault plane solutions and scalar seismic moments for the largest earthquakes provide the description of the average strain rate tensor. The principal strain rate axes show a dominant extension in NE-SW direction, a SE-NW direction of compression and a negligible thickening rate. *P* and *T* axes direction of the smaller earthquakes suggests that the same mode of deformation is distributed all over the activated volume. These results are discussed in terms of seismic deforming processes active at the Alban Hills volcano, in the frame of magmatic inflation recently invoked to explain the rapid vertical uplift affecting part of the volcano. The observed average deformation is consistent with shear failures occurring on faults connecting stress-oriented dykes in response to an increasing fluid pressure.

Key words *seismic moment release – average strain rate tensor – Alban Hills volcano*

1. Introduction

The Alban Hills are one of the main volcano craters of the peri-Tyrrhenian belt which started erupting 0.7 Ma ago (De Rita *et al.*, 1988). The magmatic activity ended about 0.027 Ma with a phreatomagmatic phase that formed numerous craters in the south-western part of the volcano. Hydrothermal phenomena, vertical uplift (up to 30 cm in the past 40 years; Amato and Chiarabba, 1995), and seismicity, testify to a residual activity of the volcano.

Mailing address: Dr. Giulio Selvaggi, Istituto Nazionale di Geofisica, Via di Vigna Murata 605, 00143 Roma, Italy; e-mail: selvaggi@marte.ingrm.it

In recent and historical times, seismicity has been characterised by long low-magnitude seismic swarms, that can last for years, concentrated close to the area where the most recent phreatomagmatic phase took place. This is also the area of rapid vertical uplift (Amato and Chiarabba, 1995). The occurrence of seismic swarms has been interpreted as a response to distributed deformation in roof rocks produced by a deeper inflating magma chamber (Chiarabba *et al.*, 1997). From a kinematic point of view, the arching of top layers should result in a relevant dip slip component in the fault plane solutions. This is true if seismic deformation approximates, in shape and not necessarily in amplitude, the total deformation of the Alban Hills volcano as a whole (see Jackson, 1993, for a discussion on the relation between faulting and continuous deformation).

In this paper, we estimated the shape of the average strain rate tensor within the seismogenic volume of the Alban Hill Quaternary

volcano, activated during the last seismic swarm (Amato *et al.*, 1994) which occurred in 1989-1990, by summing moment tensors of the largest events. Our goal is to see how the deformation produced by the discontinuous motion on faults, expressed by the average seismic strain rate tensor, is related to the mostly aseismic continuous processes, testify by the vertical uplift.

2. Method and data

Determination of the seismic strain tensor provides a major constraint on seismotectonic reconstruction within a deforming region (Jackson and McKenzie, 1988; Ekström and England, 1989; Amelung, 1996). Seismic strain tensor can be obtained from a combination of scalar seismic moment and fault plane solutions of earthquakes occurring in a given volume (Kostrov, 1974). This technique has been used in several active deforming regions, where large, moderate and micro-earthquakes occur. The well known Kostrov's formula relates the cumulative seismic moment tensor M_{ij}, in a volume (V) during a time window t, with the average strain-rate tensor ($\dot{\bar{\varepsilon}}_{ij}$), in the following way:

$$\dot{\bar{\varepsilon}}_{ij} = \frac{1}{2\mu V t} \sum_{k=1}^{N} M_{ij}^{k}.$$

Strain is highly dependent on the referenced volume. The volume activated during the 1989-1990 swarm was imaged by the spatial distribution of seismic moment release. In these maps the symbolic representation of the earthquake size is substituted by seismic moment distribution interpolated over a square grid cell.

The Istituto Nazionale di Geofisica deployed a temporary digital local network during the last seismic swarms from April 1989 until the beginning of 1990 (Amato *et al.*, 1994). The digital network was composed of four three-component short period digital stations, one broadband weak motion station and seven short-period vertical component stations, that recorded the one-year-long seismic swarm from its beginning. Four accelerometers triggered for the largest events. More than one thousand earthquakes, out of the three thousand recorded, were located by Amato *et al.* (1994). Figure 1a,b shows the network geometry and the distribution of the best located events (horizontal and vertical errors of the events in fig. 1a,b are less than 2 km). Location accuracy is described in Amato *et al.*'s (1994) paper, which also identified a shallow structure 12 km long, 3 km wide and 3 km thick where the seismicity occurred during the swarm.

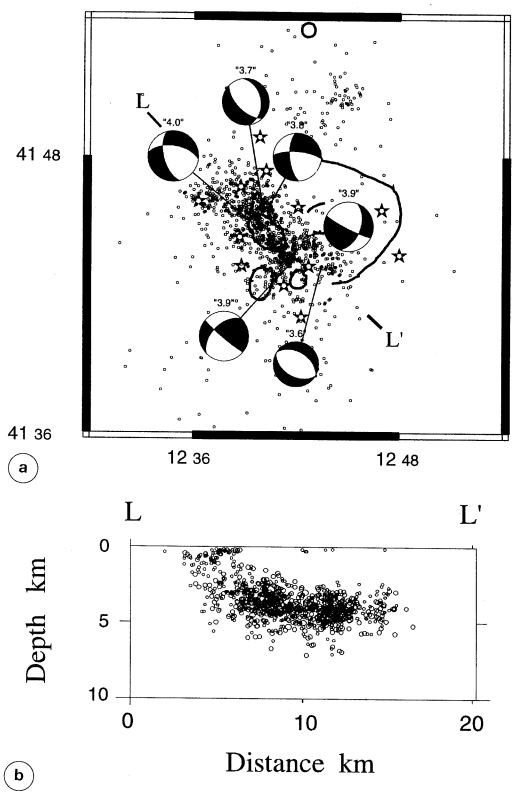

Fig. 1a,b. a) Epicentral map of the 1989-1990 earthquake swarm at the Alban Hills volcanic complex. Errors on the location are less than 2 km both in horizontal and vertical plane. Also shown are the fault plane solution of the largest earthquakes which occurred during the sequence. Stars indicates station locations. b) Longitudinal section of the swarm.

3. Seismic moment distribution

Our data set contains location and duration magnitude (M_d) of all the earthquakes of the seismic swarm. We sought a linear empirical relation between the logarithm of seismic moment and magnitude, calibrated for the Alban Hills region, to calculate the seismic moment of all the earthquakes.

Seismic moments were estimated from the low frequency amplitudes of the *S*-wave displacement spectra, for 23 selected events, recorded at the weak motion broadband, 125 sps digital station in the magnitude range 1.4 ÷ 2.9. Larger magnitude events clipped the weak motion sensor, and for the four $M_L > 3.9$, the seismic moments were calculated from the *S*-wave acceleration spectra, recorded at the strong motion stations (Chiarabba, 1993). There is a lack of information between magnitude 3.0 and 3.9 due to the clipping of the weak motions above $M = 3.0$ and a lack of triggers below $M = 3.9$ for the strong motions. For these 27 events we also determined the local magnitude and the duration coda magnitude. The estimates of seismic moment, local magnitude and duration magnitude allowed us to determine the coefficients of the linear relation between Log (M_o) and M_L or M_d, in the magnitude range between 1.4-4.5 (fig. 2a,b), the latter being the largest event of the sequence. The two equations are explicit in the following form:

$$\text{Log } (M_o) = \\ = 1.032\ (\pm 0.003)\ M_L + 17.489\ (\pm 0.008) \tag{3.1}$$

$$\text{Log } (M_o) = \\ = 1.505\ (\pm 0.008)\ M_d + 16.1\ (\pm 0.2). \tag{3.2}$$

Relation (3.1) is correlated with a coefficient equal to 0.99, while (3.2), although the data are more scattered, still provides an acceptable correlation (0.97). We used relation (3.2) to estimate the seismic moment for all those earthquakes for which we have only the duration magnitude. The total seismic moment release, calculated over the complete seismic sequence, is $8.8 \cdot 10^{22}$ dyne · cm, equivalent to a single $M_w = 4.6$. Figure 3 shows the cumulative time

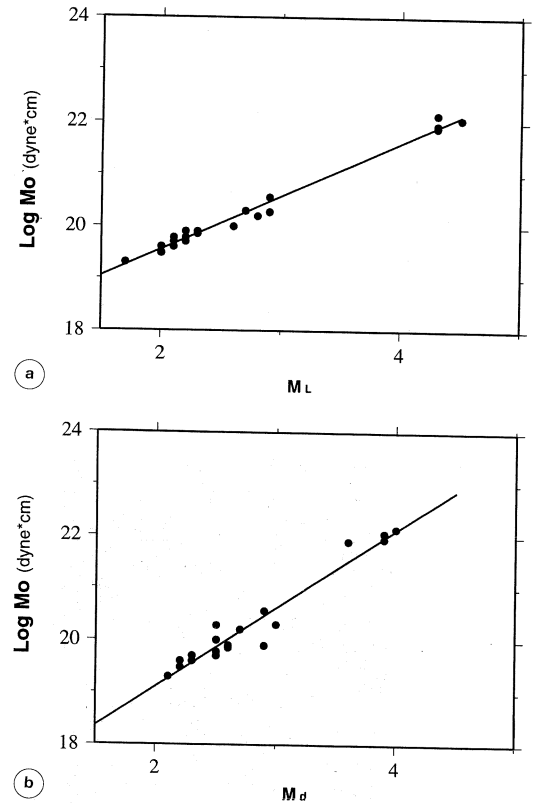

Fig. 2a,b. Linear regressions between Log (M_o) and M_L (a); M_d (b). Regression coefficients are equal to 0.99 and 0.97 for (a) and (b), respectively.

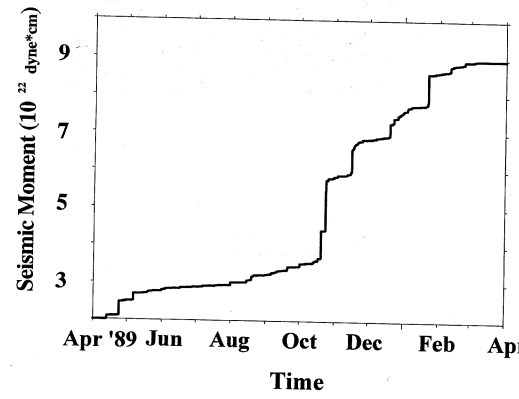

Fig. 3. Cumulative time distribution of scalar seismic moment.

distribution of the earthquake swarm. The first part of the sequence, characterised by a large number of earthquakes, has a low rate of moment release. Since October 1989, moment rate has increased sharply and it is dominated by the occurrence of 5 larger earthquakes.

To portray seismic release, we divided the area into square cells of 0.5 km × 0.5 km. The seismic moment of all the earthquakes falling into the same cells are summed up and represented in their cumulative value. Figure 4a,b shows an interpolated image of the seismic moment release both in map and in depth. Such a representation better shows the area where the significant release occurred. The activated structure is imaged as a ~ 3 km wide belt striking NW-SE for about 7 km. The seismic moment release at depth is shown in the section LL′. The depth interval below 3 km has been the most active with a sharp cut-off of seismicity at 5 km depth.

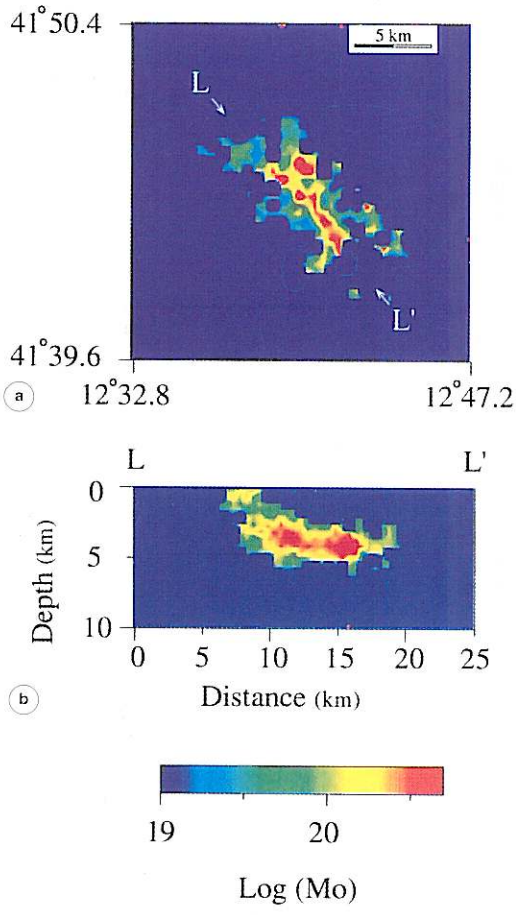

Fig. 4a,b. Seismic moment distribution: a) map view; b) longitudinal section.

4. Seismic strain

More than 50% of the total scalar seismic moment of the seismic sequence was released by only six events, out of the one thousand located, for which strike, dip and rake of the fault plane solutions (Amato *et al.*, 1994), and the seismic moment, are available. The complete description of the moment tensor can be obtained by a combination of fault plane solutions and the scalar seismic moment (Aki and Richards, 1980). The fault plane solutions are for normal and strike slip faults (fig. 1a,b), all showing an extensional T axis approximately sub-horizontal, inclined towards NE-SW, while P axes are slightly scattered in different azimuths and plunge. Each component of the moment tensors is summed and the resulting moment tensor provides a fault plane solution with a main strike slip component (fig. 5a,b). T axis is subhorizontal and its direction is consistent with the direction of the regional extension, deduced from fault plane solutions and borehole breakout (Amato *et al.*, 1995, Montone *et al.*, 1996). The P axis is NW-SE striking and has a plunge of 35°.

The strain rate tensor was obtained considering the volume derived from seismic moment distribution (7 km × 3 km × 3 km) and a time window of one year. Table I shows the component of the strain rate tensor in geographic coordinates ($\dot{\bar{\varepsilon}}_{11}$ is in NS direction, $\dot{\bar{\varepsilon}}_{22}$ in EW direction and $\dot{\bar{\varepsilon}}_{33}$ along Z). The principal strain rate axes show that the average deformation is extension in NE-SW direction, compression in NW-SE and a negligible deformation along the depth axis (table II).

Fault plane solutions are also available for smaller earthquakes (Chiarabba, 1993). Al-

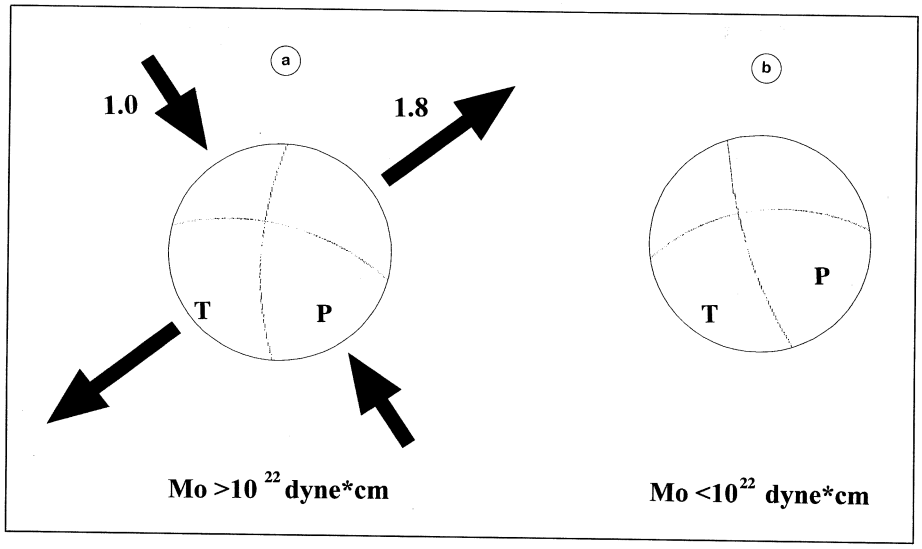

Fig. 5a,b. Resulting fault plane solution after moment tensor summation. a) Solution obtained from the six largest events (strike 185°, dip 71°, rake −30°). Also indicated are the horizontal principal axes direction of the strain rate tensor and their length in 10^{-14} s^{-1}. b) Solution obtained from smaller earthquakes (strike 184°, dip 53°, rake − 29°).

Table I. Component of the strain rate tensor ($\dot{\bar{\varepsilon}}_{11}$ is in NS direction, $\dot{\bar{\varepsilon}}_{22}$, in EW direction and $\dot{\bar{\varepsilon}}_{33}$ along Z).

Average strain rate tensor	$\dot{\bar{\varepsilon}}_{11}$	$\dot{\bar{\varepsilon}}_{12}$	$\dot{\bar{\varepsilon}}_{13}$	$\dot{\bar{\varepsilon}}_{22}$	$\dot{\bar{\varepsilon}}_{23}$	$\dot{\bar{\varepsilon}}_{33}$
(10^{-14} s^{-1})	− 0.14	1.3	0.09	0.9	− 0.40	− 0.76

Table II. Azimuth, plunge and length of the principal strain rate axes.

Principal strain rate axes	$\dot{\bar{\varepsilon}}_1$	$\dot{\bar{\varepsilon}}_2$	$\dot{\bar{\varepsilon}}_3$
Azimuth-plunge	142 35	115 55	237 6
Length (10^{-14} s^{-1})	− 1.2	− 0.6	1.8

though the quality of these solutions is poorer than for the largest events, they are more of them, providing almost a complete analysis of the average seismic deformation during the swarm. The moment tensor obtained from the summation of the smaller earthquakes shows nearly the same solution derived from the largest one (fig. 5a,b). Moreover, P and T axes direction suggests that the same mode of deformation is distributed all over the activated volume (fig. 6). Only the direction of a small number of P and T axes (grey axes in fig. 6), in the central part of the phreatomagmatic craters, implies extension and compression in opposite direction with respect to the one derived from the average strain rate tensor.

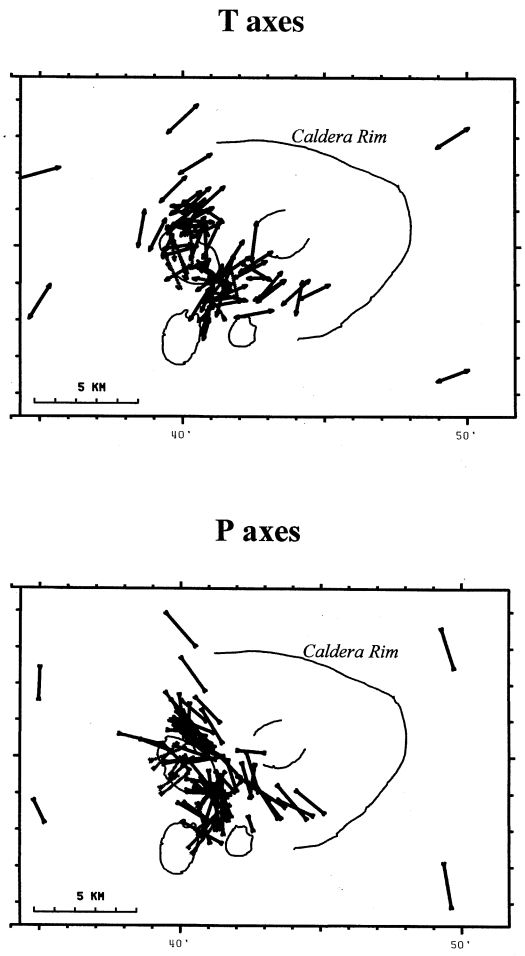

Fig. 6. *T* and *P* axes distribution of smaller earthquakes. Light grey arrows are axes with different azimuth with respect to the principal direction observed from the largest earthquakes.

5. Discussion and conclusions

Chiarabba *et al.* (1997) proposed an evolution model for the Alban Hills volcano that explains much of the geophysical evidence collected in past years, particularly tomographic images (Cimini *et al.*, 1994), rapid vertical uplift and seismicity distribution. The model is based on present-day accumulation of magma at depth below approximately 6 km. The inflation of the magma chamber is also responsible for the observed vertical uplift, that is the main deformation process of the area. In this framework, seismicity is activated by the arching or bending of the upper layers in response to the deeper inflation (Chiarabba *et al.*, 1997). In our paper we show that the seismic deformation is confined to a 7 km long, 3 km wide and 3 km thick volume and the average seismic strain rate is most likely related to horizontal relative motion (see table I). The main seismic deformation is extension in NE-SW direction in agreement with the regional extension direction. Compression in NW-SE direction also has a large component, while the thickening rate is negligible. The distribution of *P* and *T* axes of the small magnitude earthquakes suggests that the same mechanism is sheared in the whole activated area.

Such mode of crustal deformation is not peculiar to the Alban Hills volcano. A common feature of volcanic areas, like Long Valley caldera or Phlegraean Fields, is the large vertical uplift combined with moderate seismic release. The deformation produced, or better accommodated, by many swarm-like sequences is not directly related to uplift or collapse mechanism, but rather it shows a predominant horizontal motion characterised by strike slip faulting. An explanation for this deformation field is the geometric model shown in Hill (1977). It consists of two main points: a) cluster of magma-filled or fluid-filled dykes within brittle volumes of the crust; oriented in a regional deviatoric stress field perpendicular to σ_3; b) oblique fault planes connecting adjacent tips of offset dykes. If the fluid pressure in the dykes increases up to σ_3, the stress field within the volume will reach a critical state. Shear failures occurring on the oblique faults give rise to the seismic swarm that will last until the entire volume is again in equilibrium. An equivalent mechanism is achieved when regional tectonic stress increases. The swarm develops when the volume reaches the critical state due to the passive inflation of fluid or magma in the dykes at a pressure equal to σ_3. The observed average strain at the Alban Hills volcano is consistent with the physical model for earthquake swarms of Hill (1977).

Finally, we have shown that earthquake size can be efficaciously represented on maps in terms of scalar seismic moment, providing original images of seismic activity.

Acknowledgements

We thank D. Giardini and an anonymous referee for their constructive criticisms that greately improved the original manuscript. We also thank A. Amato and C. Chiarabba for helpful suggestions.

This work has been partially founded by ASI-ARS contract 1997.

REFERENCES

AKI, K. and P. RICHARDS (1980): *Quantitative Seismology* (W.H. Freeman and Company, San Francisco), p. 117.

AMATO, A. and C. CHIARABBA (1995): Recent uplift of the Alban Hills volcano (Italy): evidence for magmatic inflation?, *Geophys. Res. Lett.*, **22**, 1985-1988.

AMATO, A., C. CHIARABBA, M. COCCO, M. DI BONA and G. SELVAGGI (1994): The 1989-1990 seismic swarm in the Alban Hills volcanic area, Central Italy, *J. Volcanol. Geotherm. Res.*, **61**, 225-237.

AMATO, A., P. MONTONE and M. CESARO (1995): State of stress in Southern Italy from borehole breakout and focal mechanism data, *Geophys. Res. Lett.*, **22**, 3119-3122.

AMELUNG, F. (1996): Kinematics of small earthquakes and active tectonic and topography in the San Francisco Bay region, *Ph. D. Thesis.*

CHIARABBA, C. (1993): Caratteri sismologici dell'area vulcanica dei Colli Albani, *Pubbl. Int.*, 548 (in Italian).

CHIARABBA, C., A. AMATO and P.T. DELANEY (1997): Crustal structure, evolution, and volcanic unrest of the Alban Hills, Central Italy, *Bull. Volcanol*, **59**, 161-170.

CIMINI, G.B., C. CHIARABBA, A. AMATO and H.M. IYER (1994): Large teleseismic *P*-wave residuals variation in the Alban Hills volcano, Central Italy, *Ann. Geofis.*, **37** (5), 969-988.

DE RITA, D., R. FUNICIELLO and M. PAROTTO (1988): Geological map of the Colli Albani volcanic complex («Vulcano Laziale»), *CNR-GNV, Joint venture ENEA-AGIP.*

EKSTRÖM, G. and P. ENGLAND (1989): Seismic strain rates in regions of distributed continental deformation, *J. Geophys. Res.*, **94**, 10231-10257.

HILL, D.P. (1977): A model for earthquake swarms, *J. Geophys. Res.*, **82**, 1347-1352.

JACKSON, J. (1993): Relations between faulting and continuous deformation on the continents, *Ann. Geofis.*, **36** (2), 3-11.

JACKSON, J. and D. MCKENZIE (1988): The relationship between plate motion and seismic moment tensor, and the rates of active deformation in the Mediterranean and Middle East, *Geophys. J.*, **93**, 45-73.

KOSTROV, V.V. (1974): Seismic moment and energy of earthquakes, and seismic flow of rock, *Izv. Acad. Sci. USSR Phys. Solid Earth*, **1**, 23-44.

MONTONE, P., A. AMATO and M.T. MARIUCCI (1996): The state of stress in the Italian peninsula, in *Proceedings EGS The Hague, May, 1996.*

(received April 6, 1998;
accepted June 19, 1998)